communications biology

Article

https://doi.org/10.1038/s42003-024-06801-6

Alkaloids of Aconiti Lateralis Radix Praeparata inhibit growth of non-small cell lung cancer by regulating PI3K/Akt-mTOR signaling and glycolysis

Wen Zhang[1,2,4] ✉, Shuhui Cai[1,2,4], Lihong Qin[1,2,4], Yaru Feng[1,2], Menglei Ding[1,2], Zichen Luo[1,2,3], Jinjun Shan[3] & Liuqing Di[1,2] ✉

Aconiti Lateralis Radix Praeparata (*Fuzi* in Chinese) is widely used in the clinical treatment of tumors. This study aims to explore the active fractions and underlying mechanisms of *Fuzi* in the treatment of non-small cell lung cancer (NSCLC). *Fuzi* alkaloids (FZA) is prepared and found to inhibit the growth of NSCLC both in vitro and in vivo significantly. A total of 53 alkaloids are identified in FZA by UPLC-Q-TOF-MS. Proteomics experiment show that 238 differentially expressed proteins regulated by FZA are involved in amino acid anabolism, pyrimidine metabolism and PI3K/Akt-mTOR signaling pathway. Metabolomics analyses identify 32 significant differential metabolites which are mainly involved in amino acid metabolism, TCA cycle and other pathways. Multi-omics research combined with molecular biological assays suggest that FZA might regulate glycolysis through PI3K/Akt-mTOR pathway to treat NSCLC. The study lays a foundation for the anti-cancer investigation of *Fuzi* and provides a possible scientific basis for its clinical application.

Lung cancer is the most commonly diagnosed carcinoma worldwide and associated with a high mortality rate[1]. Non-small cell lung cancer (NSCLC), accounting for approximately 85% of lung cancers, remains a low cure and survival rate due to its high recurrence and metastasis[2,3]. Existing clinical treatment of NSCLC mainly includes surgery, radiotherapy, chemotherapy, targeted therapy and immunotherapy[4]. However, surgery and radiation are used in advanced NSCLC cancer patients. Chemotherapy and radiotherapy are often accompanied with side effects, such as fatigue, nausea, and gastrointestinal reactions. Furthermore, molecular targeting treatment is prone to drug resistance[5]. Traditional Chinese medicine (TCM) could improve the patients' life quality, relieve their symptoms, and have a good safety profile[6]. Therefore, it is of great significance to explore TCM for the treatment of NSCLC.

Aconiti Lateralis Radix Praeparata (*Fuzi* in Chinese) is the processed daughter or lateral root of *Aconitum carmichaelii* Debx.[7]. It was firstly recorded in *Agriculture God's Canon of Materia Medica* that *Fuzi* has the effect of treating tumors. *Fuzi* is frequently employed in clinical practice to treat lung cancer, gastric cancer, and other malignant tumors[8–10]. The famous *Fuzi*-based formulas, including Sini Decoction, Mahuang Fuzi Xixin Decoction, Shenfu Injection and Compound Sansheng Injection[11–13], exert excellent therapeutic effects in anti-cancer treatment. Modern studies indicated that the components in *Fuzi*, such as aconitine, hypaconitine, mesaconitne and higenamine, exhibited anticancer functions[14–18]. However, these studies on *Fuzi* are mostly focused on monomer components. Our previous research reported that *Fuzi* decoction had a significant inhibitory effect on tumor growth[19]. Meanwhile, the active components and the underlying mechanism of *Fuzi* decoction in NSCLC treatment remains elusive.

Proteomics study is a systematic investigation of differences in protein expression levels, modification status, interactions, quantities, and characteristics in the process of disease occurrence and drug treatment, which is widely used to clarify the mechanism of TCM[20]. Metabolomics research comprehensively expounds the mechanism of drugs by analyzing the change of the metabolite in the organism under normal physiological and pathological conditions, which is a key method for pharmacological study[21]. Metabolomics is widely regarded as the omics discipline closest to phenotype with the identification and quantification of small-molecule metabolites, by comparing the systematic differences in metabolites between different experimental groups and revealing their inherent laws.

[1]School of Pharmacy, Nanjing University of Chinese Medicine, Nanjing, China. [2]Jiangsu Engineering Research Center for Efficient Delivery System of TCM, Nanjing, China. [3]Jiangsu Key Laboratory of Pediatric Respiratory Disease, Institute of Pediatrics, Nanjing University of Chinese Medicine, Nanjing, China. [4]These authors contributed equally: Wen Zhang, Shuhui Cai, Lihong Qin. ✉e-mail: wenzhang@njucm.edu.cn; diliuqing@njucm.edu.cn

Metabolomics is not only a descriptive indicator of phenotype, but can also affect the physiological function by regulating genomics, transcriptomics, proteomics, and other multiple omics[22]. The joint analysis of differential proteins with metabolic pathways were conducted in order to find their relevance and study of upstream and downstream regulatory pathways of proteins and metabolites through proteomics screening of differential proteins, metabolomics identification of differentially expressed metabolites and metabolic pathways[23]. Meanwhile, through constructing drug-disease targeting networks, network pharmacology has been widely used to predict the active ingredients, therapeutic targets and signaling pathways to reveal the potential mechanism of TCM[24]. To sum up, multi-omics technology combined with network pharmacology could investigate the underlying molecular mechanism of TCM more comprehensively and systematically, in line with its multi-component, multi-pathway and multi-target characteristics.

Cell metabolic reprogramming is a pivotal marker of malignant tumors[25]. The Warburg effect is a metabolic feature of cancer cells, which consume lots of glucose and produce lactate to satisfy the growing demand for energy and biosynthetic requirements under aerobic conditions[26]. Researchers revealed that cancer cells used the Warburg effect to maintain the activity of the PI3K signaling pathway, thus promoting glycolytic metabolism to ensure the continuous growth and division of cancer cells[27,28]. The PI3K/Akt-mTOR signaling pathway is involved in regulating a variety of cellular physiological processes by activating the corresponding downstream effectors, which plays a key role in tumor proliferation, invasion and metastasis[3,29]. When PI3K is activated, it catalyzes the phosphorylation of phosphatidylinositol 4,5-bisphosphate (PIP2) to form phosphatidylinositol 3,4,5-trisphosphate (PIP3). Then PIP3 recruits 3-phosphoinositide-dependent protein kinase-1 (PDK1) and Akt proteins to the plasma membrane, leading to phosphorylation of Akt by PDK1[30]. Phosphorylated Akt inhibits the kinase activity of glycogen synthase kinase-3 beta (GSK-3β), preventing Cyclin D1 degradation, thereby regulating glucose metabolism. Akt activation could enhance glucose uptake in cancer cells through regulation of glucose transporter-1 (GLUT1)[28]. In addition to enhancing glucose uptake, Akt regulates several glycolytic enzymes such as hexokinase 2 (HK2) and phosphofructokinase (PFK) through post-translational and transcriptional mechanisms[31]. PI3K-dependent Akt activation results in enhanced PFK2 phosphorylation and production of fructose-2,6-bisphosphate, which in turn promotes PFK1 activation. The enhanced PI3K/Akt-dependent PFK1 activation and GLUT1 expression promoted the Warburg effect, cell proliferation, and tumorigenesis[32]. Activation of mTORC1 could promote elevated levels of hypoxia inducible factor-1 (HIF-1α), leading to the induction of aerobic glycolysis in tumor cells[33]. Activated mTORC1 could also have an effect on the expression levels of glycolysis-related enzymes in tumor cells through the regulation of downstream transcription factors. These findings underscore the instrumental role of PI3K/Akt-mTOR in regulating metabolism. Accordingly, regulating tumor metabolism by targeting PI3K/Akt-mTOR pathway has become a therapeutic strategy for cancers.

In this study, *Fuzi* alkaloids (FZA) and *Fuzi* polysaccharides (FZP) were extracted and purified from *Fuzi* firstly. The xenograft mice model was used to evaluate the anti-NSCLC effect of *Fuzi*, FZA and FZP. After that, ultra-performance liquid chromatography quadrupole time-of-flight mass spectrometry (UPLC-Q-TOF-MS) was employed to analyze the chemical composition of the effective fraction. Moreover, TMT-based proteomics, non-targeted metabolomics and network pharmacology were applied to investigate the active ingredients and molecular mechanism against NSCLC. Lastly, the related mechanism was verified by assay kits, gas chromatography-mass spectrometry (GC-MS) analyses and western blotting experiment.

Results

FZA inhibited NSCLC growth both in vivo and in vitro

To further assess the anti-cancer effects of FZA and FZP in vivo, the A549 xenograft mice were administrated with PBS, 15 g/kg FZ, 2 g/kg FZA, 7.5 g/kg FZP daily, 4 mg/kg cisplatin as positive control every two days for 14 days. Compared with the model group, the growth rate of nude mice in the treatment group slowed down (Fig. 1A). Notably, mice administrated with FZA showed significantly smaller tumor volume relative to mice of model group. As shown in Fig. 1B, it was observed that mice belonging to the FZA group exhibited the most significant inhibition of tumor weight at the end of the experiment. The anti-tumor effect of FZA was significant, and the tumor inhibition rate was up to 70.98%. These results showed that FZA had a comparable efficacy to that of the positive control cisplatin group, while FZP showed a fairly weak tumoricidal activity. In addition, H&E staining on tumor sections from the model group showed a dense arrangement of tumor cells, regular morphology and large volume, with high nucleoplasm ratio and less division, accompanied by a small number of lymphocytes and neutrophil infiltration, which could be significantly alleviated following the treatment of FZ, FZA, FZP (Fig. 1D). Moreover, no significant weight loss (Fig. 1C), or any other obvious signs of toxicity was observed in the hearts, spleens, lungs, livers, or kidneys after FZA administration (Fig. 1E, F). These suggests that FZA and FZP have low toxicity in these mice.

Furthermore, to characterize the anti-cancer potential of FZA in vitro, the cytotoxicity against five NSCLC cell lines including A549, NCI-H1975, NCI-H1299, NCI-H460 and NCI-H1650 cells were assessed. As shown in Fig. 1G, FZA showed significant tumoricidal activity in all five tested NSCLC cell lines with 22.41–139.57 μg/mL IC_{50} values. Besides, NSCLC cell viability significantly decreased by FZA in a time and concentration dependent manner (Fig.1H). Above all, the results suggested that FZA was able to inhibit NSCLC growth both in vivo and in vitro.

Component identification of FZA

Through the in vivo and in vitro studies, FZA was identified as the effective fraction of *Fuzi* in treatment of NSCLC. Six batches of FZA were prepared and the content of main alkaloids were measured. The average contents of main alkaloids of FZA including benzoylmesaconitine (BMA), benzoylaconitine (BA), benzoylhypaconitine (BHA), mesaconitine (MA), and hypaconitine (HA) in six batches of FZA were 837.58 ± 29.19, 80.21 ± 3.56, 19.15 ± 0.77, 34.43 ± 2.90, 53.92 ± 4.06 μg/g, respectively (Table S1). The results indicated that the preparation method of FZA was stable (Fig.S1). In order to further reveal the composition of FZA, the chemical profiling of FZA was investigated by UPLC-Q-TOF-MS at the positive ion modes. The total ion chromatograms (TICs) were presented in Fig. 2A, B. The structural elucidation of chemical ingredients with the accurate mass measurement of quasi-molecular within 5 ppm error was performed based on the data of available reference compounds, chromatographic retention times, and MS/MS data or its associated literatures. A total of 53 compounds in FZA were identified, mainly including diester-diterpenoid alkaloids (DDAs) monoester-diterpenoid alkaloids (MDAs), and aminoalcohol-diterpenoid alkaloids (ADAs). In positive ion mode, acetyl, benzoyl, methoxy and hydroxyl groups were possible substituents on the skeleton of diester-diterpenoid alkaloids, shown in Fig. 2C. The accurate mass measurements for the protonated molecular ions of the 53 constituents in FZA in positive ion mode were summarized in Supplementary Data 2. Retention times, formulas, experimental and theoretical masses, mDa and ppm errors were included.

Proteomics analysis

To further explore the exact mechanism underlying the inhibitory effect of FZA on NSCLC growth, the multiplexed TMT-based quantitative proteomics strategy was employed to profile the changed proteins in A549 tumors treated with FZA. Briefly, A549 tumors treated with FZA or PBS were lysed, and proteins were digested by trypsin. The generated peptides were labeled with TMT reagents followed by high-pH reversed-phase HPLC fractionation and then analyzed by LC-MS/MS (Fig. S2A). As a result, a total of 6166 proteins were identified, of which 6143 proteins were quantified across all the 6 samples. Furthermore, quality of proteomic data sets and instrumental reproducibility were evaluated (Fig. S2B–2E). In the principal component analysis (PCA) plot, samples were separated into two groups obviously according to different treatments (Fig. S2F). Moreover, as shown

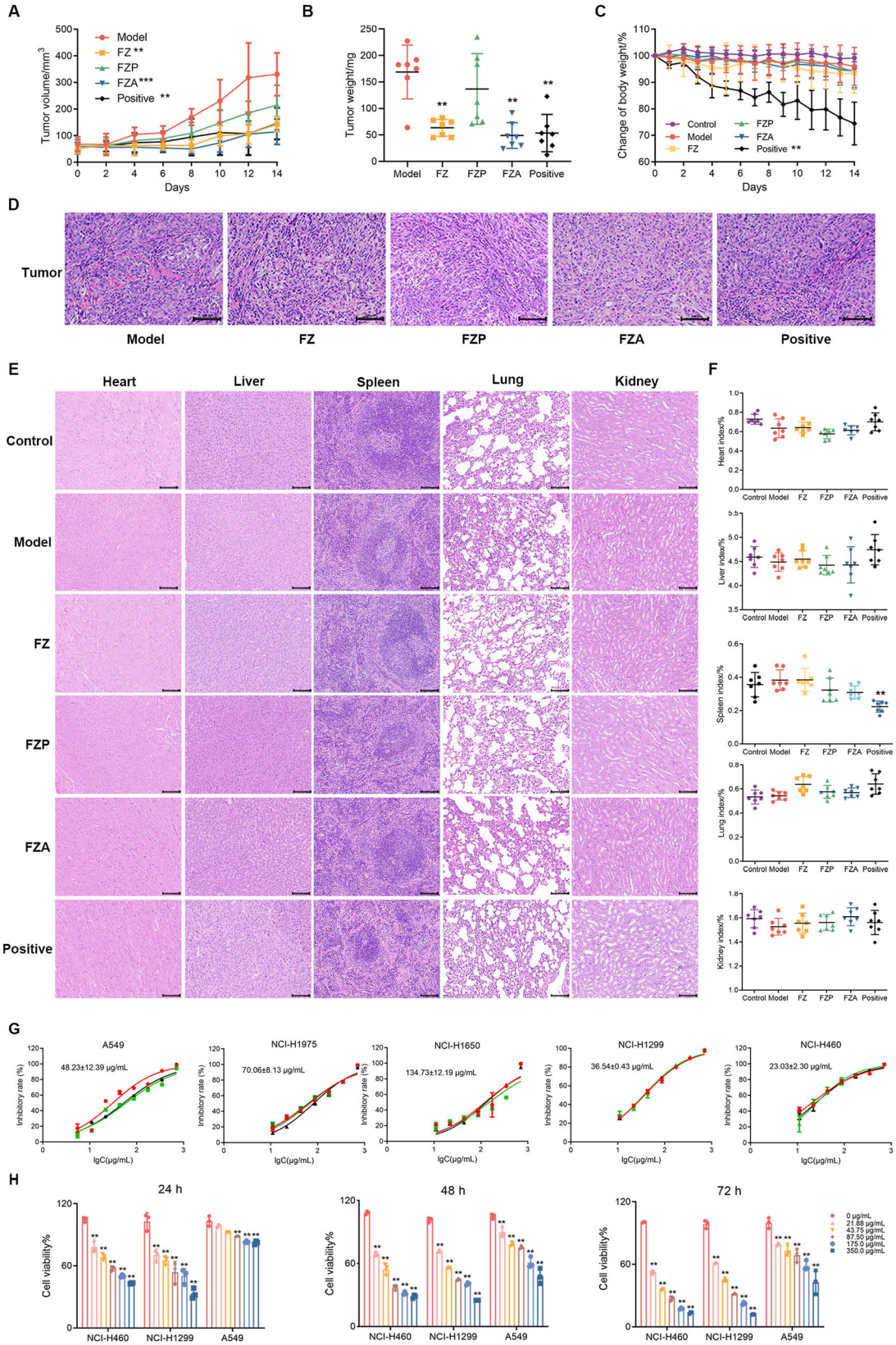

Fig. 1 | FZA inhibited NSCLC growth both in vivo and in vitro. A Tumor volume growth curves of the mice. **B** Tumor weight of the mice at the end of the experiment. **C** Changes in body weight of the mice. **D** H&E staining of the tumor sections. **E** Histological analysis of the major organs slices after treatments. The scar bar was 100 μm. **F** The viscera indexes of lung, heart, spleen, liver, kidney of the mice were calculated. **G** The cytotoxic activities of FZA against NSCLC cells for 72 h. IC_{50} value were evaluated by Graph Prism. The red line, green line, and black line respectively represented the first, second, and third time of MTT experiment. ($n = 3$) (H) Cell viability assay treated with different doses of FZA ($n = 3$). Data were presented as the mean ± SD. Error bars indicated SD. $^{*}p < 0.05$, $^{**}p < 0.01$; $^{***}p < 0.001$. All data were from three independent experiments.

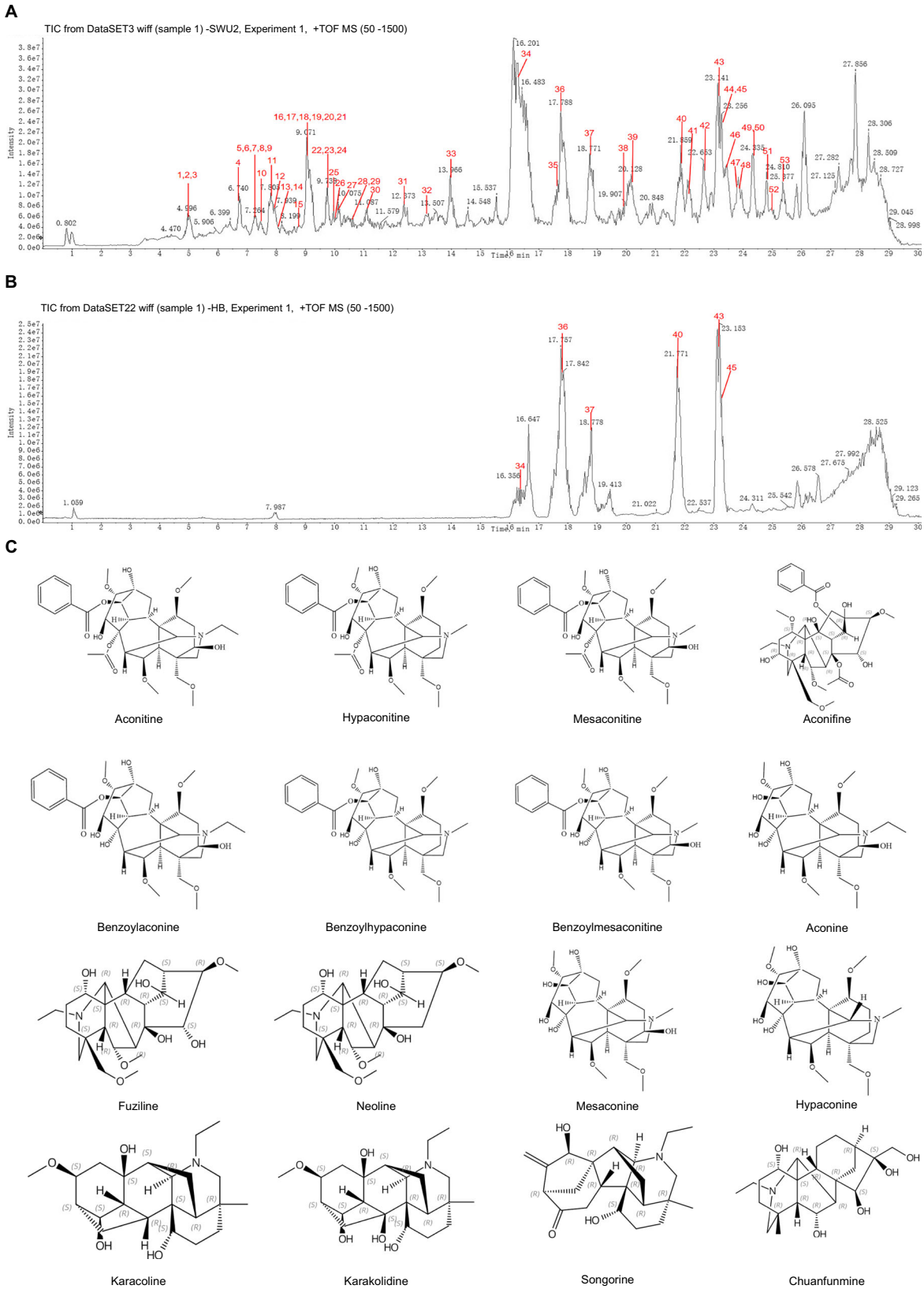

Fig. 2 | Component identification of FZA by UPLC-Q-TOF-MS. A Total ion current chromatogram of FZA. **B** Total ion current chromatogram of the mixed reference substances. **C** Structures of the representative ingredients in FZA.

in Fig. S2G, CV cumulative curve displayed a smaller coefficient of Variance between each sample, suggesting good reproducibility of the biological replicates. Taken together, these results demonstrated that the TMT-based proteomic analysis provided a high-quality and reproducible dataset. Next, the significantly changed proteins were filtered with the criteria of fold change >1.2 and p value < 0.05. This resulted in 132 up-regulated and 106 down-regulated proteins in the FZA group (Fig. 3A, Supplementary Data 2). Hierarchical clustering was used to cluster the differentially expressed

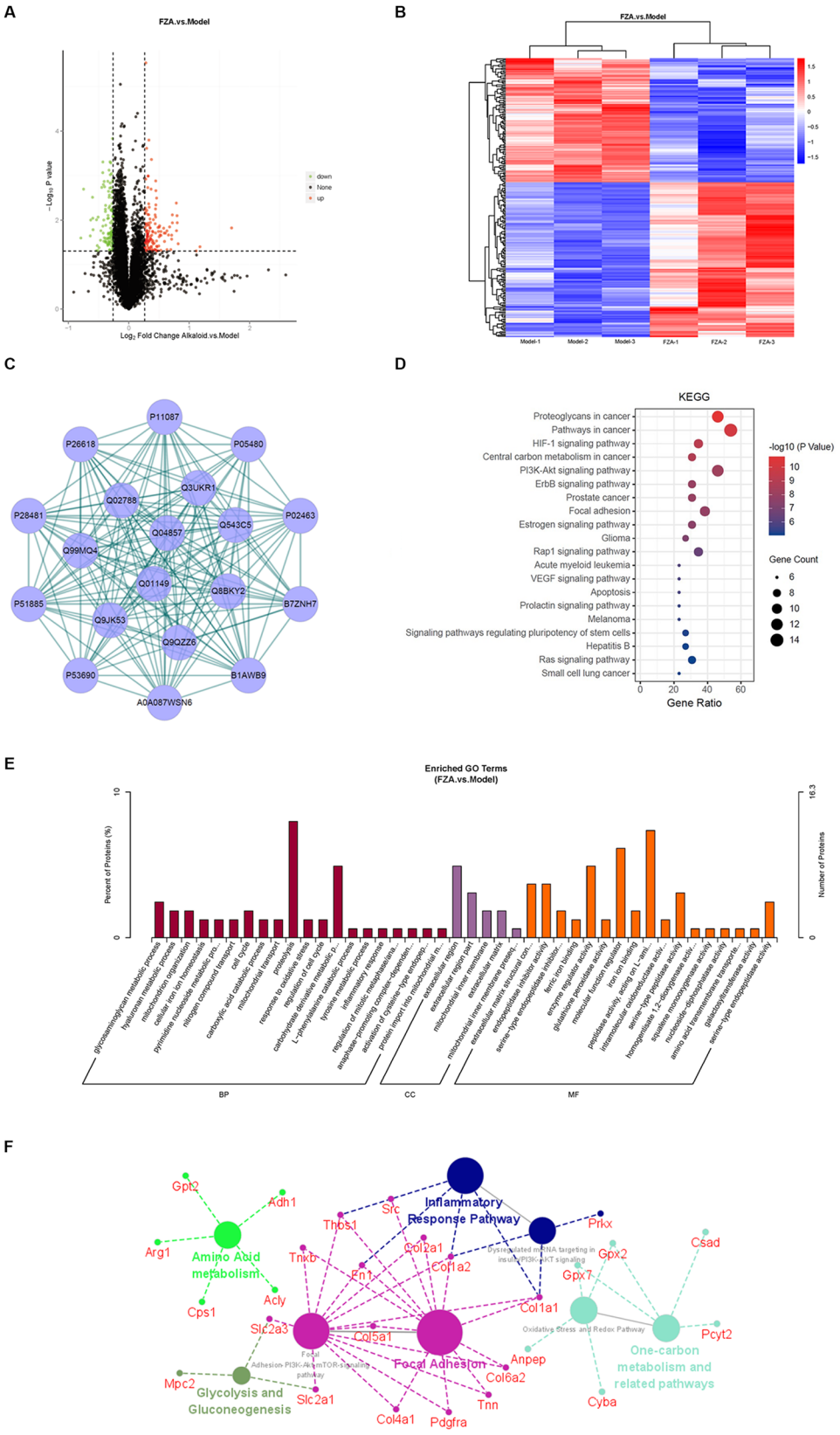

Fig. 3 | The mechanism of FZA in treatment of NSCLC was analyzed by TMT-based proteomics. **A** The volcano plot showed the upregulated (red) and downregulated (green) proteins between FZA and model groups. **B** Hierarchical cluster analysis of 238 DEPs. The colors indicated fold changes of the proteins, the blue color indicated an increase while red indicated a decrease. **C** The top 20 core genes were analyzed by MCODE. **D** KEGG pathways of FZA against NSCLC. The gradual color represented the *P* value and the size of the black spots represented the gene number enriched in the pathways. **E** GO analysis of the 238 DEPs in biological process, cellular component, and molecular function respectively. **F** The key proteins were uploaded to the CluoGO plug-in of Cytoscape for analyzing biological processes.

proteins between the two groups. Figure 3B showed that three samples of FZA group were clustered into one group, and the samples of the model group were clustered into another group, indicating the protein expression of FZA group was different from that of the model group.

To understand the biological characterization of these proteins, the 238 differentially expressed proteins were imported into the STRING database (https://string-db.org/) and constructed a PPI network (Fig. S2H). The networks for highly connected regions were analyzed using the Cytoscape (plugin, MCODE), which indicated that the top 20 core genes may play key roles in FZA effect against NSCLC (Fig. 3C). The DEPs were categorized according to the following GO classes: biological process, molecular function, and cellular components. Gene Ontology (GO) and Kyoto

Encyclopedia of Genes and Genomes (KEGG) analysis were further carried out to identify the biological pathways associated with FZA antitumor activity. These results showed that the DEPs were predominantly localized in the extracellular matrix and mitochondria, which mainly affected the activity of diverse enzymes and participated in tumor metabolism processes (Fig. 3E). KEGG analysis further identified that the DEPs were mainly enriched in PI3K/Akt-mTOR, central carbon metabolism in cancer, glycolysis/gluconeogenesis, taurine and hypotaurine metabolism, arginine metabolism, tyrosine metabolism, arachidonic acid metabolism, pyrimidine metabolism, and metabolic pathways (Fig. 3D). Furthermore, the DEPs were used for pathway analysis by CluoGO plugin. The results mainly also involved the PI3K/Akt-mTOR, central carbon metabolism in cancer, and glycolysis/gluconeogenesis (Fig. 3F).

Metabolomics analysis

To investigate the metabolic influence of FZA, differential metabolites in plasma samples from NSCLC mice were analyzed by non-targeted metabolomics analysis. To start with, the total ion chromatography of serum samples from the control, model, and FZA groups showed that the peak shapes were good and the distribution was relatively uniform under the test conditions (Fig. S3A). Next, PCA was used to analyze the quality control data, and the PCA score plot exhibited that there were clear separations among the different groups (Fig. 4A). The results indicated that xenotransplantation of tumor induced changes of endogenous metabolites in nude mice while FZA reversed this change. PLS-DA and OPLS-DA were both better applied to show that FZA group was significantly separated from the model group (Fig. S3B). Furthermore, FZA group was separated from the model group and much closer to the control group, which highlighted the anti-NSCLC effects of FZA (Fig. 4B).

Based on the outcome of LC-MS/MS and the information from the online database, the identification of these metabolites was carried out. The heat-maps vividly showed differential metabolites in serum. The difference between the FZA group and the model group indicated that FZA exerted a certain regulatory effect on the abnormal levels of metabolites in xenograft mice (Fig. 4C). As listed in Table S2, compared with the model group, 32 metabolic biomarkers changed after treatment with FZA. FZA was found to have the potential to normalize the abnormal levels of various metabolites associated with the inflammatory response. These metabolites included beta-alanine, glucose-6-phosphate, aspartate, proline, fumarate, ornithine, glycine, malate, uracil, threonine, lysine, aconitic acid, and several others. The results suggested that FZA may exert its anti-NSCLC effects by regulating the content of these metabolites. In addition, pathway enrichment analyses were conducted using the KEGG database to explore the mechanisms of action further. The MetaboAnalyst database were also applied to calculate the *p*-value and the pathway impact value based on pathway enrichment. These analyses helped to identify the specific metabolomic pathways involved in the anti-NSCLC effects of FZA. According to pathway impact and *p*-value, the potential pathways associated with the effect of FZA anti-NSCLC were finally identified. The identified biomarkers and related pathways were shown in Fig. 4D. The findings pointed mainly to the involvement of beta-Alanine metabolism, Arginine biosynthesis, Pyrimidine metabolism, TCA cycle, Glyoxylate and dicarboxylate metabolism, Starch and sucrose metabolism, Arginine and proline metabolism, Glycolysis and gluconeogenesis. The differential metabolites in metabolomics analysis were imported into the software of Cytoscape 3.8.2 to construct the compound-reaction-enzyme-gene networks using the plugin of Metscape. As shown in Fig. 4E, FZA might exerts its anti-NSCLC effects by regulating the TCA cycle and glycolysis.

Integrated analyses of the proteomics and metabolomics results

Further integrated analyses of the proteomic and metabolomic studies exhibited that the altered pathways in response to FZA were likely to rectify expressions of proteins and metabolites involved in energy metabolic pathways. The molecular action network of differential proteins and metabolites was established to explain the relationship between differential proteins and metabolites, with TOP10 biological pathways enriched, including central carbon metabolism, amino acid anabolic metabolism, glycolysis, TCA cycle purine metabolism, glycine, serine and threonine metabolism, glyoxalate and dicarboxylic acid metabolism, glutathione metabolism, urea cycle, arginine and proline metabolism (Fig. 5A). Furthermore, the Pearson correlation analysis of the relationship between proteomics and metabolomics was performed by "Wu Kong" platform (https://www.omicsolution.com/wkomics/main/). The targets of FZA were mainly concentrated in central carbon metabolism, amino acid anabolism, glycolysis, TCA cycle, purine metabolism and other pathways closely related to energy metabolism (Fig. 5B). Above all, we speculated that FZA exerted its anti-NSCLC effect by regulating tumor energy metabolism.

Network pharmacology prediction

Anti-cancer effect of FZA on NSCLC was confirmed by our in vivo and in vitro experimental data. Based on the complexity of TCM ingredients and the integrity of their effects, FZA might exert anti-tumor effects through multi-component, multi-target, and multi-pathway, which is consistent with the systematic view of network pharmacology. Totally 210 potential treatment targets of FZA and 1040 target genes of NSCLC were identified, among which 34 key targets intersected (Fig. 6A). PPI analysis concluded that FZA acted on core targets such as AKT1, EDFR, SRC, BCL2, MTOR, KDR, PI3KCA, KIT, and PARP1, as shown in Fig. 6B. The drug-ingredient-target-disease network was constructed with 90 nodes and 168 connecting edges (Fig. 6C). Subsequently, GO enrichment analysis of these 34 core targets were performed to explore the potential therapeutic mechanisms of FZA in NSCLC. Moreover, KEGG pathway enrichment analysis showed the most significantly enriched 20 pathways of FZA involved in NSCLC in Fig. 6D. The pathways in cancers showed the largest number of involved targets (17 counts), followed by the PI3K/Akt signaling pathway. The analysis revealed that FZA acted on NSCLC mainly through biological processes such as PI3K/Akt signaling regulation, protein phosphorylation and transmembrane receptor protein tyrosine kinase signaling pathway (Fig. 6E). Based on the above results, we speculated that FZA might treated NSCLC by regulating tumor energy metabolism *via* PI3K/Akt signaling pathway.

FZA regulated aerobic glycolysis through the PI3K/Akt-mTOR pathway

Based on the results of proteomics, metabolomics and network pharmacology experiments, we speculated that FZA played an anti-NSCLC role by regulating tumor energy metabolism. To verify the hypothesis, the glucose and lactate kits were used to detect the ability of cell glycolysis. As shown in Fig. 7A, the lactate contents in A549 and NCI-H1299 cells were reduced and the pH values of the cultured medium were elevated, suggesting that FZA had an inhibitory effect on lactate production in NSCLC cells. Meanwhile, it was found that the intracellular glucose content of A549 and NCI-H1299 cells increased after FZA treatment. Furthermore, the contents of citrate, isocitrate, α-ketoglutarate, succinate, fumarate and malate were increased, indicating a certain recovery of TCA cycle (Fig. 7B). The results suggested that the metabolic pathway was diverted from glycolysis to oxidative phosphorylation after treatment with FZA. To elucidate how FZA suppressed aerobic glycolysis in NSCLC cells, several key enzymes involved in the regulation of glycolytic pathways were examined, including glucose transporter 1 (GLUT1) and lactate dehydrogenase A (LDHA). However, the protein expressions of GLUT1 and LDHA were not significantly changed (Fig. 7C).

Interestingly, it was found that FZA dose-dependently inhibited the expressions of p-PI3K, p-Akt, and p-mTOR, without influencing total levels of PI3K, Akt, and mTOR (Fig. 7D). The ratios of p-PI3K/PI3K, p-Akt/Akt, and p-mTOR/mTOR reduced with statistical significance as show in Fig. 7E. These observations support that FZA might regulate the Warburg effect of NSCLC cells by affecting PI3K/Akt-mTOR pathway. To further confirm the regulatory role of FZA on the PI3K/Akt-mTOR signaling pathway, A549 cells were treated with the inhibitor of PI3K, LY294002. Compared with the control group, the cell viability in the FZA group, LY294002 group, combined group were decreased to 60.8%, 65.5%, or 56.8% respectively (Fig. 7F).

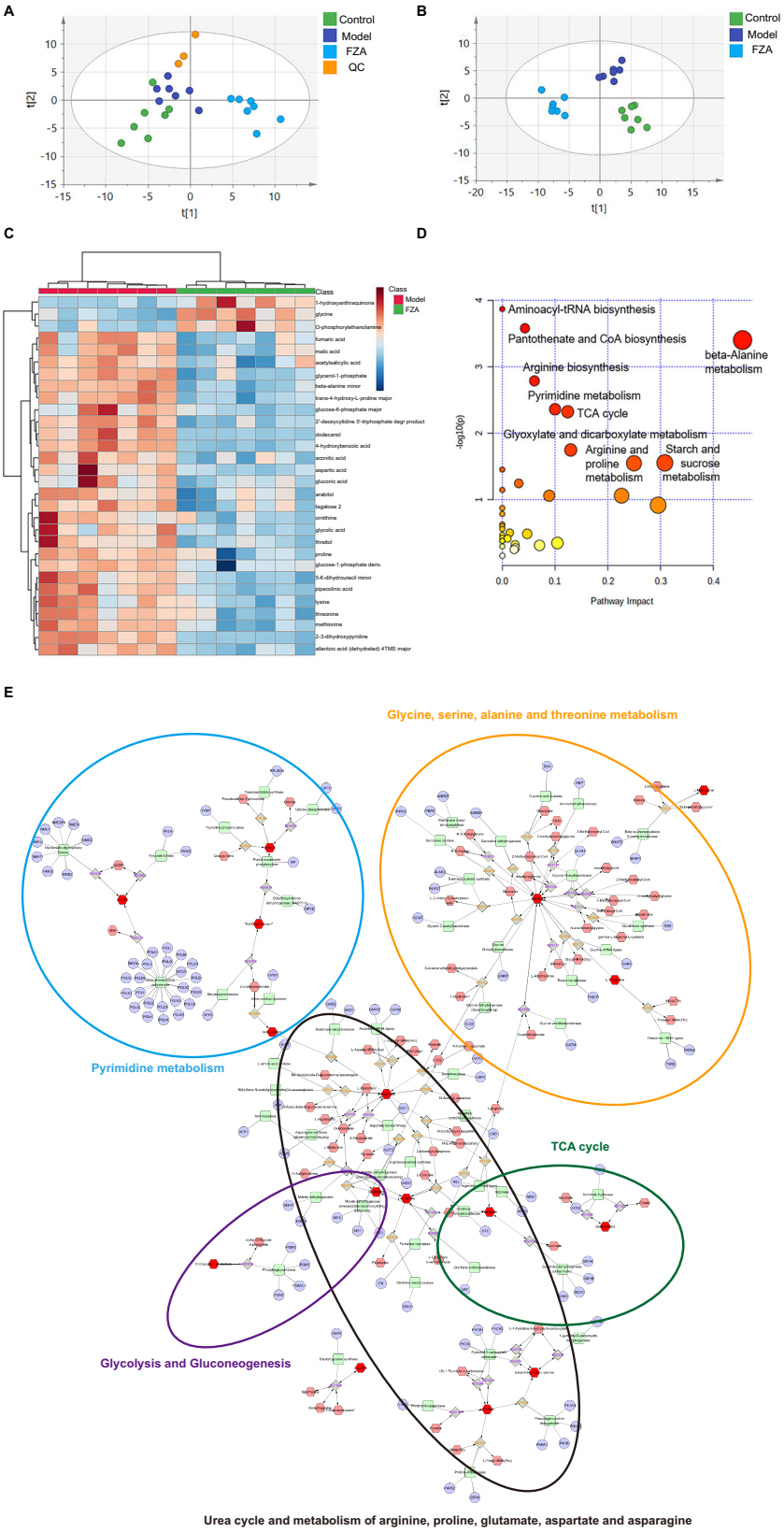

Fig. 4 | The mechanism of FZA in treatment of NSCLC was investigated by non-targeted metabolomics. A PCA scores scatter plot of serum metabolites. **B** PLS-DA scores scatter plot of serum metabolites. **C** Heatmap showed the differentially expressed metabolites between Model and FZA groups with adjusted *P* value < 0.05, $|Log_2FC| > 0.58$ (Up-regulation metabolites were presented as red dots, whereas the down-regulation ones were in blue). **D** Pathway enrichment analysis by the MetaboAnalyst 4.0 tool. The y-axis represented the *p* value and the x-axis represented the impact value. The pathways were represented as a text-based on the *p* value. The color and size of each circle represent *p*-value and pathway impact values, respectively. **E** The compound-reaction-enzyme-gene networks of the key metabolites and targets. The compounds, reactions, enzymes, and genes were represented by the light red hexagons, gray squares (with associated KEGG reaction identifier numbers), green rounded corner squares, and light blue circles (with associated gene symbols), respectively. The input potential metabolites were represented by red hexagons.

The cell viability of the 2-hour pre-treatment group with LY294002 was lower than FZA treatment group. Compared with the FZA group, the cell viability of the combination group was significantly reduced ($p < 0.05$). The MTT assay showed that inactivation of PI3K/Akt-mTOR enhanced the inhibitory effect of FZA on A549 cell proliferation. Furthermore, compared with the control group, it was found that FZA and LY294002 inhibited the proteins expression of p-PI3K and p-Akt respectively. However, the inhibitory effect of FZA on the protein levels of p-PI3K and p-Akt was intensified by the addition of LY294002 (Fig. 7G). Taken together, it could be concluded that these findings verified the hypothesis got from the multi-omics research and network pharmacology that FZA may treat NSCLC by regulating glycolysis *via* the PI3K/Akt-mTOR pathway.

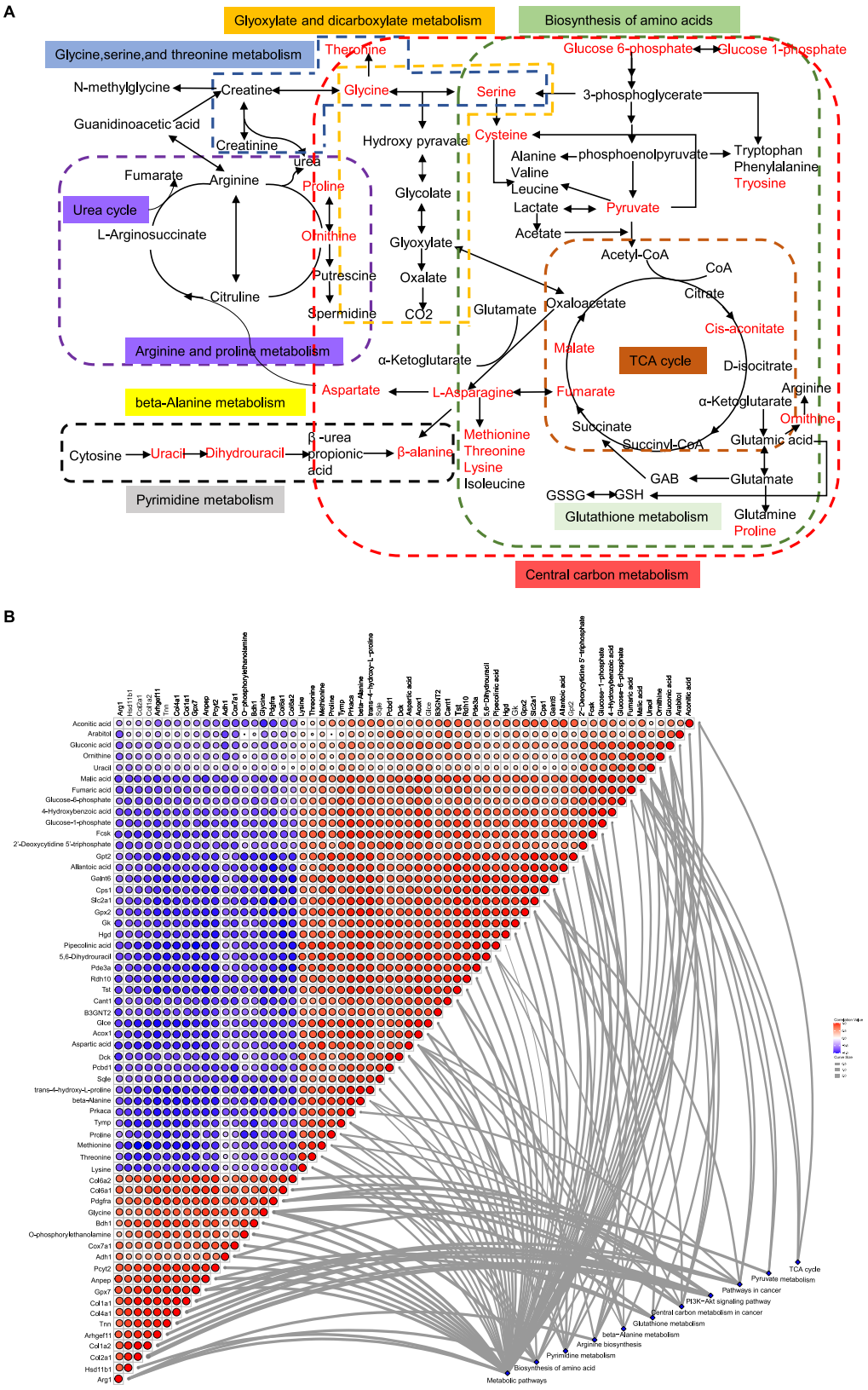

Fig. 5 | Integrated analyses of the proteomics and metabolomics results. **A** Enriched pathways of proteomics and metabolomics combined analysis. Visualization of the molecular interaction network of differential proteins and metabolites was conducted by associating 238 differential proteins and 32 differential metabolites. The metabolic pathways jointly involved in differential proteins and metabolites were screened. **B** The Pearson correlation analysis of the correlation between the proteomics and metabolomics experiment. The colors of the circles indicated the values associated with each metabolite and protein. The red grid indicated positive correlation, while the blue grid indicated negative correlation. The darker the color was, the higher the correlation value was. The thickness of the gray curve indicated the contribution degree of each protein and metabolite to related pathways. The relationships between different proteins, different metabolites and pathways were clearly reflected through correlation analysis.

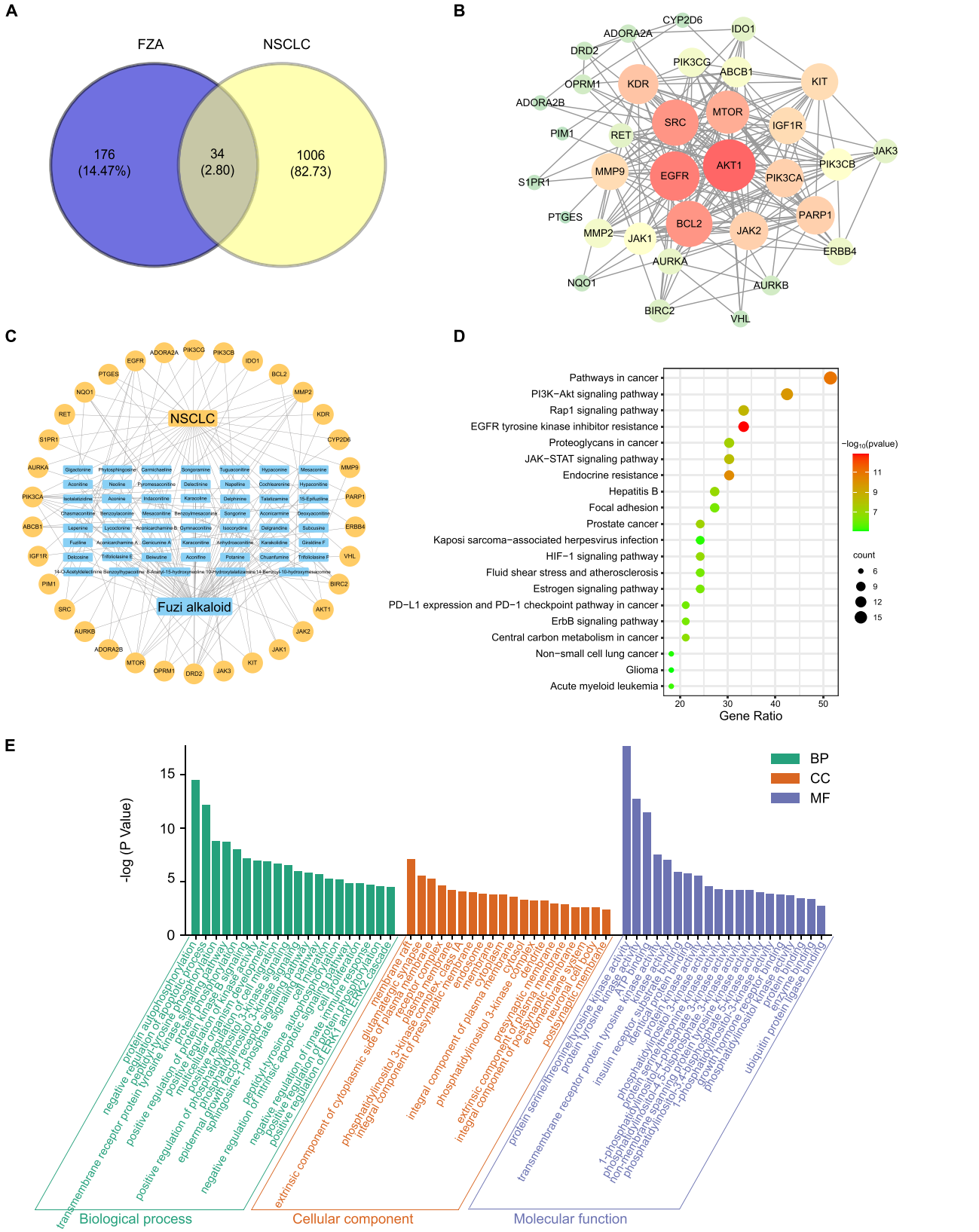

Fig. 6 | The mechanism of FZA on NSCLC was predicted by network pharmacology. A Intersection analysis between FZA targets and the disease genes of NSCLC. **B** PPI network analysis. The PPI network has 90 nodes and 168 edges. **C** The drug-ingredient-target-disease network illustrated the interaction between ingredient of FZA and NSCLC-targeted genes. The blue square box indicated ingredient of FZA, while the orange circles indicated NSCLC target. **D** KEGG pathway analysis showed that FZA had an effect on the biological processes in treatment of NSCLC. **E** Gene ontology analysis on the involvement of major biological process and molecular function of common genes regulated by FZA on NSCLC.

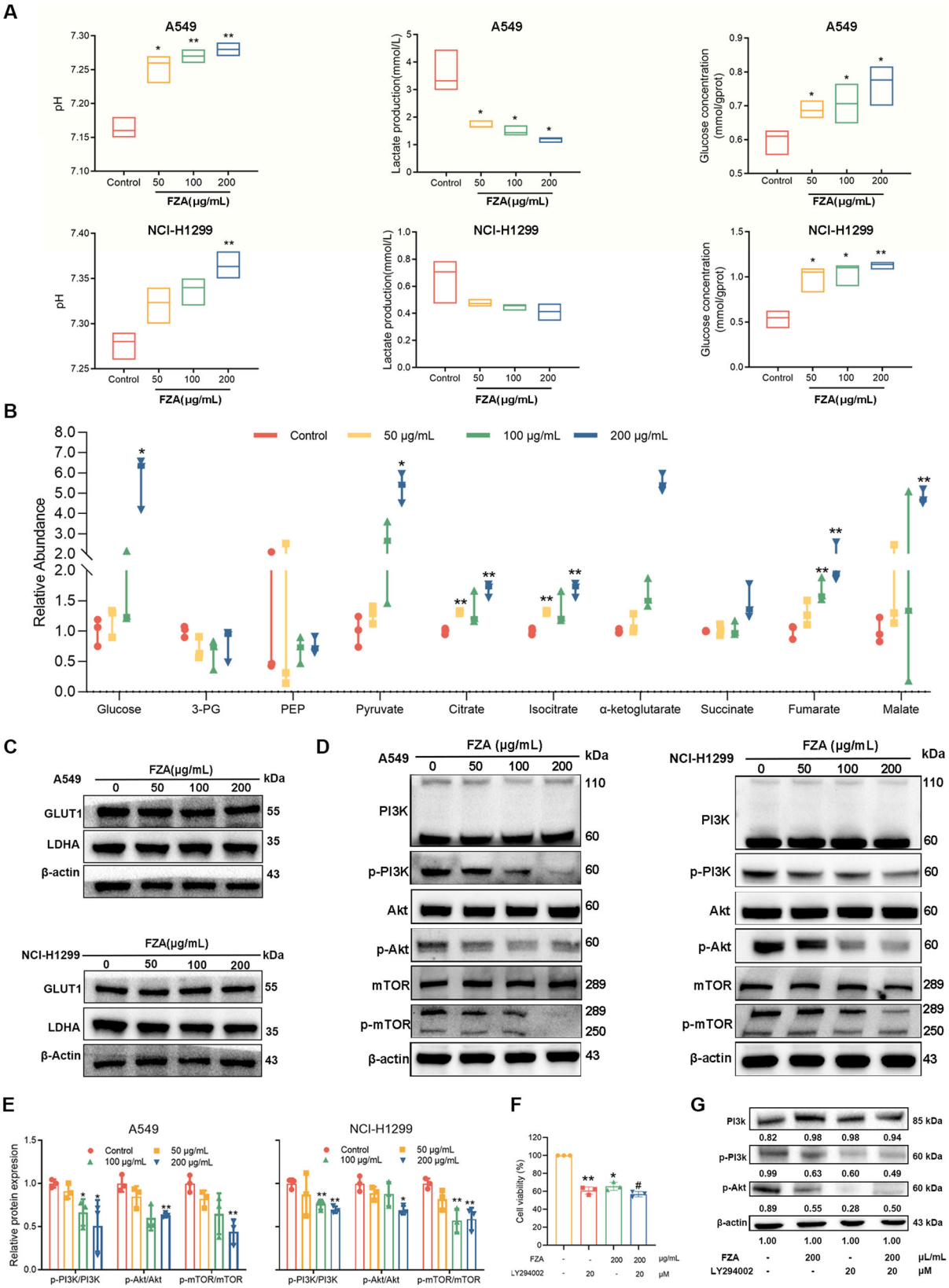

Discussion

NSCLC is one of the leading causes of cancer-related deaths around the world, its prevention and treatment remain a major clinical challenge[34]. Numerous clinical practices have revealed the wisdom of the use of TCM, so there is an increasing attention on TCM formulations, herbs, and their active ingredients in anti-cancer research[35]. Our previous experiments have revealed that *Fuzi* decoction possessed profound anti-NSCLC effects in vivo, which showed good safety at effective doses[19]. However, the anti-NSCLC effect of the major constituent of *Fuzi* remained unknown. In this study, FZA was extracted and purified from *Fuzi*, and 53 alkaloid components

Fig. 7 | FZA regulated aerobic glycolysis in NSCLC cells. A NSCLC cells were treated with FZA (0, 50, 100, and 200 μg/mL) for 24 h. Intracellular glucose and lactate content were detected ($n = 3$). **B** GC-MS was utilized to measure intracellular glucose, 3-phosphoglycerate, PEP, pyruvate, citrate, isocitrate, α-ketoglutarate, succinate, fumarate, and malate in A549 cells ($n = 3$). **C** Influence of FZA on Glycolysis related kinase protein expression of GLUT1 and LDHA in NSCLC cells ($n = 3$). **D** NSCLC cells were treated with various concentrations of FZA for 24 h. Protein levels of PI3K, p-PI3K, Akt, p-Akt, mTOR, p-mTOR, and β-actin were detected. β-actin was served as control. **E** Quantification of band intensity is shown on the right bar chart ($n = 3$). **F** The effect of FZA combined with LY294002 on the proliferation of A549 cells. All data were from three independent experiments. **G** The effect of FZA combined with LY294002 on the protein levels of PI3K, p-PI3K, and p-Akt of A549 cells. Data were presented as the mean ± SD. Error bars indicated SD. $^{*}p < 0.05$, $^{**}p < 0.01$ versus control by one-way ANOVA and post hoc tests$^{\#}$, $p < 0.05$ versus the concentration of 200 μg/mL FZA. The ratios of the level of PI3k, p-PI3k, or P-Akt relative to actin was indicated underneath each corresponding band in the figure. The densitrometric analysis presented in the figure was on a single replicate.

were identified by UPLC-Q-TOF-MS qualitative analysis. It was found that FZA significantly inhibited tumor growth with little toxic and side effects in the A549 xenograft mice model. MTT tests showed that FZA possessed strong anti-NSCLC activity.

Unlike normal cells, regardless of the oxygen content, pyruvate in tumor cells is mainly converted to lactate to produce ATP, thus maintaining sufficient macromolecular synthetic substrates for the proliferation of active tumor cells, this phenomenon is known as Warburg effect[36,37]. The underlying mechanism of Warburg effect is complex and involves activation of oncogenes, inactivation of tumor suppressor genes, abnormal expression of glycolytic enzymes and alterations in the tumor microenvironment[26]. The regulation of glycolytic products is part of metabolic reprogramming and is closely related to the occurrence and development of tumors. Therefore, glycolytic metabolism is becoming more and more important in the study of anti-tumor treatment. To fully grasp the biological effects of FZA, proteomics and metabolomics were used to investigate the pathways of action. The changes in proteins after FZA administration were illustrated by TMT-based proteomics analyses. Differential metabolites and metabolic pathways were identified by metabolomics, and the overall regulatory role of FZA was accordingly elucidated. The results showed that the targets of FZA were mainly enriched in amino acid synthesis and metabolism, glutathione metabolism, lipid metabolism, suggesting that FZA might play an anti-NSCLC role by regulating cellular metabolism. Furthermore, assay kits verified that FZA reduced glucose consumption and lactate production in tumor cells as well as targeted metabolomics analysis showed that FZA increased the content of TCA cycle-related products, indicating that FZA rectified the metabolic pathway from glycolysis to oxidative phosphorylation. All in all, it showed that FZA rectified the metabolic pathway from glycolysis to mitochondrial respiration and accordingly treated NSCLC.

Through the network pharmacology analysis, it was found that FZA treated NSCLC mainly through the Pathways in cancer, PI3K/Akt-mTOR signaling pathway and Central carbon metabolism. The PI3K/Akt-mTOR pathway is one of the most pivotal regulatory pathways of Warburg effect in malignant tumor cells[38]. Previous clinical studies have found that upregulation of the PI3K/Akt-mTOR pathway are common in NSCLC patients[39]. Similarly, it was reported that β-elemene suppressed tumor metabolism of NSCLC by regulating PI3K/Akt-mTOR signaling[40]. Combining multi-omics and network pharmacology, it was supposed that FZA might inhibit the growth of tumor cells by regulating glycolysis *via* PI3K/Akt-mTOR signaling pathway. To verify this hypothesis, western blotting analyses showed that FZA suppressed the phosphorylation levels of PI3K, Akt, and mTOR, without influencing the protein expression of PI3K, Akt and mTOR. Hence, we suggested that FZA might exert antitumor effects by inhibiting PI3K/Akt-mTOR signaling, which could be an effective measure to block NSCLC development. Further research would be needed to investigate the specific active ingredients of FZA and their precise pharmacological targets.

Conclusions

In summary, a total of 53 alkaloid components were identified in FZA, which was extracted and purified from *Fuzi*. The results suggested that FZA inhibited the growth of NSCLC in vitro and in vivo by regulating glycolysis through PI3K/Akt-mTOR signaling pathway. Our results thus highlight FZA as a potential therapy for NSCLC that might exert anticancer effects by regulating the PI3K/Akt-mTOR signaling pathway.

Materials and methods

Reagents and antibodies

F-12kaighn's (F12k) modification medium, RPMI modification medium, pancreatin, penicillin-streptomycin, and phosphate-buffered saline (PBS) were purchased from Hyclone Laboratories, Inc. (Logan, UT, USA). Fetal bovine serum was obtained from Gibco (Grand Island, NY, USA). Dimethyl sulfoxide (DMSO) was acquired from Sinopharm Chemical Reagent Co., Ltd. (Shanghai, China). Cisplatin was purchased from Aladdin Biochemical Technology Co., Ltd. (Shanghai, China). TMT®Mass Tagging Kits and Reagents was sourced from Thermo Fisher Scientific (Waltham, MA, USA). The glucose assay kit and lactic acid assay kit were purchased from Jiancheng Bioengineering Institute (Nanjing, China). PI3K (4249S), phospho-PI3K (4228S), Akt (4691S), phospho-Akt (4060S) and phospho-mTOR (5536S) antibodies were purchased from Cell Signaling Technology Inc. (Beverly, MA, USA). Lamin B1(12987-1-AP), beta-actin (20536-1-AP), mTOR (20657-1-AP) and HRP-conjugated Affinipure Goat Anti-Rabbit IgG(H + L) (SA00001-2) were obtained from Proteintech Group, Inc. (Chicago, USA). LY294002 (PI3K inhibitor) was bought from TargetMol Chemicals Inc. (Shanghai, China). The other chemicals and reagents were analytical grade and commercially available.

Preparation of Fuzi decoction, FZA and FZP

The preparation process of *Fuzi* decoction was stated as follows. *Fuzi* was obtained from Bozhou Yonggang Pharmaceutical Co., Ltd (Sichuan, China) and was authenticated by Professor Shengjin Liu (Nanjing University of Chinese Medicine, Nanjing, China). *Fuzi* was mixed with eight times the amount of water and boiled for one hour. The resulting liquid was collected by passing it through a filter, and the solid residue was subjected to the same process again. The liquid obtained from the second extraction was then combined with the first one using filtration. The combined liquid was then concentrated to obtain the final extract.

FZA was prepared according to our previous publication, in which the extraction and purification method was optimized by central composite design-response surface methodology[41].The process of FZA was summarized as follows. After *Fuzi* pieces had been beaten into powder, the *Fuzi* powder was soaked in 4-fold 85% ethanol for 24 h and filtered. The residue was added with 4 times 85% ethanol solution and extracted by heating at reflux 4 times, each time for 2 h. After the residue was washed with small quantity of ethanol, the impregnating solution, extracting solution and washing solution were combined. The mixture was evaporated in vacuum to remove ethanol, and distilled water was added to obtain the loading solution. 50 mL of 0.16 g/mL sample solution was taken and eluted with D101 macroporous resin using distilled water, 80% ethanol respectively. Lastly, the extracts were dried into powder by vacuum freeze-dried technology.

The preparation method of FZP was generalized as follows. After extraction of FZA, the dried drug residue was subjected to ultrasonic extraction for twice with 4-fold ultrapure water, each time for 1 h. The extract was combined and concentrated appropriately, 95% ethanol was added to the crude extract until the final concentration was 80%, followed by precipitating overnight at 4 °C. Next, the crude extract was filtered, and the residue was washed with absolute ethanol and acetone to obtain crude polysaccharide, further deproteinizing by using the Sevag method (trichloromethane: n-butanol = 5:1, *v/v*), shaking for 20 min and leaving in a separatory funnel for 30 min. After the solution was stratified, the chloroform-water interface was observed, and the supernatant was obtained

when a gel-like precipitate of free protein appeared. After dialysis with running water, the supernatant was precipitated with alcohol, then the sediment was washed with anhydrous ethanol and acetone. Finally, FZP was obtained by freeze drying technique.

Animal experiment

All experiment were performed in accordance with the relevant guidelines and regulations and approved by Nanjing University of Chinese Medicine. The animal procedures described in this study were approved by the Institutional Animal Care and Use Committee of Nanjing University of Chinese Medicine (approval number: 202012A008). Nude male mice (6-8 weeks) were obtained from Shanghai SLAC Laboratory Animal Co., Ltd (Shanghai, China). A549 cells at a density of 3×10^7 cells/mL in PBS were injected subcutaneously into the right axilla of nude mice. The control group was injected with 0.2 mL PBS solution at the same site. When the volume of implanted tumors reached 50 mm^3, the mice were randomized into five treatment groups and administered intragastrically with different treatments daily: PBS (10 mL/kg), FZ (15 g/kg), FZP (7 g/kg), FZA (2 g/kg). An intraperitoneal injection of 4 mg/kg cisplatin was rendered as positive control every two days. The weight of mice was recorded daily during administration and tumor volume was assessed with a vernier caliper every 2 days after inoculation. The tumor volume (V) was calculated by the following equation: V = (Maximal length × Maximal $width^2$)/2. After 2 weeks of treatment, blood was collected from eyeball venous plexus of mice, and mice were killed by cervical dislocation. To evaluate the pathological changes in the NSCLC subcutaneous xenograft mice model, the lung, heart, spleen, liver, kidney tissues, and tumor tissues were collected, fixed in 4% paraformaldehyde, followed by paraffin embedding and cutting, and stained with hematoxylin and eosin (H&E). The rest of tumor tissues was frozen in liquid nitrogen for proteomics study. The blood from the fundus venosus was set aside for 30 min, centrifuged at 1500 rpm/min for 15 min and the upper serum layer was stored in the refrigerator at −80 °C for metabolomics analysis.

Cell viability assay

The human NSCLC cell lines A549, NCI-H1975, NCI-H1650, NCI-H1299 and NCI-H460 were purchased from the cell bank of the Chinese Academic of Science (Shanghai, China). NCI-H1975, NCI-H1650, NCI-H1299 and NCI-H460 were maintained in RPMI-1640 while A549 was cultured in F12k media. The culture media were supplemented with 1% penicillin-streptomycin and 10% fetal bovine serum. The cells were cultured in 37 °C incubator equipped with 5% CO_2. Cell viability was measured by MTT assay following the manufacturer's instructions. The cells were seeded into 96-well plates (5000 cells/well) and cultured overnight, followed by treatment with different concentrations of FZA for 24 h, 48 h and 72 h.

To investigate the effect of FZA combined with LY294002 on the proliferation of A549 cells, cells were divided into four different treatments. The control group was incubated with vehicle, while FZA group was treated with 200 μg/mL FZA for 24 h and LY294002 group was treated with vehicle after 2 h of 20 μM LY294002 treatment. The combination group was administered with 20 μM LY294002 for 2 h prior to 24 h of FZA treatment. The optical density (OD) values at 490 nm were determined by a microplate reader (EnVision, PerkinElmer). IC_{50} values were calculated with Graph Prism software.

UPLC-Q-TOF-MS analysis

The freeze-dried powder was dissolved in pure methanol to prepare a solution with a concentration of 7.5 mg/mL. After vortexing, the mixture was centrifuged at 14,000 rpm for 15 minutes. Then the obtained supernatant was filtered for UPLC-Q-TOF-MS analysis. An ACQUITY UPLC system coupled with a Triple TOF™ 5600 + MS system (AB SCIEX, USA), which integrated a switchable electrospray ion source interface, was used to identify the chemical ingredients of FZA. Samples were separated on an ACQUITY UPLC® BEH C_{18} column (2.1 mm × 100 mm, 1.7 μm) at the flow rate of 0.3 mL/min along with the column temperature of 35 °C. Mobile phases A and B were 0.1% formic acid aqueous solution and pure acetonitrile, respectively. The linear gradient elution was set as follows: 0–20 min, 5% A-35% A; 20–25 min, 35%–58% A; 25–28 min, 58%–100% A; 28–29 min, 100% A; 29–30 min, 100% A. The injected volume was 5 μL. The detection wave was 235 nm. The mass spectrometry analysis was mainly performed in TOF-IDA-MS mode under the following parameters: scan range, m/z 50–1500; nebulizer gas GS1 60 psi; heater gas GS2, 60 psi; curation gas, 40 psi; temperature, 600 °C for ESI − ; ion spray voltage, 5500 eV; declustering potential, 100 eV; collision energy, 10 eV; collision energy difference, 15 eV.

TMT-based proteomic analysis

Total protein samples were extracted from frozen tumor tissue in PASP lysis buffer (100 mM NH_4HCO_3, 8 M urea, pH 8), and then quantified using a Bradford protein assay kit (Cat. P0006, Beyotime). The proteins were separated on a 12% gel by sodium dodecyl sulfate polyacrylamide gel electrophoresis and protein bands were visualized by Coomassie Blue R-250 staining. The protein solution was digested with trypsin and $CaCl_2$ at 37 °C overnight. Peptide desalination was carried out using the C_{18} desalting column, and the samples were then lyophilized following the manufacturer's instructions. The digested peptides were collected and cleaned with a C_{18} column, then the digested peptides were labeled with TMT 10-plex reagents according to the manufacturer's instructions (Thermo Fisher Scientific). The TMT-labeled peptides were dissolved in mobile phase A (98% double-distilled water, 2% acetonitrile, pH 10) and fractionated on a Waters reversed-phase BEH C_{18} column (4.6 × 250 mm, 5 μm) with a RIGOL L-3000 HPLC System. Fractions were collected one tube per minute and then dried and combined into ten fractions for further LC-MS/MS analysis. LC-MS/MS analysis was performed with an EASY-nLC 1000 System (Nano HPLC, Thermo Fisher Scientific) coupled online to a Q ExactiveTM HF-X Mass Spectrometer with a Nanospray Flex™ (ESI) Ion Source (Thermo Fisher Scientific). The LC-MS/MS raw data were processed using Proteome Discoverer 2.4 (PD 2.4, Thermo) and Uniprot database, with a false-discovery rater (FDR) < 0.01 at the level of proteins and peptides. Proteins with significant P value < 0.05 and fold change >1.2 or <0.8 were considered as differentially expressed proteins (DEPs). Based on the DEPs, Gene Ontology (GO) function analysis as well as the Kyoto Encyclopedia of Genes and Genomes (KEGG) signaling pathway enrichment analysis were carried out. Meanwhile, volcano maps and cluster heat maps were drawn to visualize differential proteins. Furthermore, the String DB (https://STRING.embl.de/) was also employed to screen DEPs and to develop protein-protein interaction (PPI) network.

Non-targeted metabolomics analysis

The serum samples stored at 80 °C were thawed on ice. After vortex mixing, 50 μL serum was placed in a centrifuge tube and 200 μL ice methanol solution containing 1,2-^{13}C-myristic acid (12.5 μg/mL) was added and vortexed for 3 min. Then the mixture was centrifuged at 18,000 r/min for 10 min at 4 °C. The supernatant was taken 100 μL and dried in a concentrator for 2 h at 45 °C. After drying, the tube was added with 30 μL methoxyamine hydrochloride dissolved in pyridine (*w/v*, 10 mg/mL), vortexed for 5 min, and oscillated in a thermostatic oscillator at 300 r/min for 90 min at 30 °C. Then 30 μL BSTFA was added and mixed. After 30 min of oscillating at 300 r/min at 37°C, the sample was centrifuged at 18,000 r/min for 10 min at 4 °C and the supernatant was performed with a GC-MS system that consisted of a Trace 1310-TSQ 8000 Evo (Thermo Fisher, San Jose, CA, USA) equipped with a TG-5MS capillary column (0.25 mm × 30 m, 0.25 μm, Thermo Fisher, San Jose, CA, USA) under the following conditions: sampling volume, 1 μL; carrier gas, helium (99.999%); flow rate, 1.2 mL/min; and split ratio, 20:1. The gradient heating program was conducted as follows: 0–1 min, 60 °C; 1–14 min, 60–320 °C; 14–19 min, 320 °C. The TSQ 8000 was equipped with an electron ionization source. The ionization energy was 70 eV, the transfer line was held at 250 °C, and the source temperature was 280 °C. The GC-MS data were acquired after a solvent delay of 3.5 min, and the MS scan range was 50-500 m/z. The GC-MS data

were converted into ABF format using the ABF Converter (http://www.reifycs.com/AbfConverter/) and imported into MSDIAL (v.4.10) software. The results were imported into SIMCA 14.1 (MKS Data Analytics Solutions, Sweden) for principal component analysis (PCA) and orthogonal projections to latent structures discriminant analysis (OPLS-DA). The MetaboAnalyst website (http://www.metaboanalyst.ca) and one-way ANOVA method were used for evaluating identified metabolites. According to $p < 0.05$, FC > 1.2 or <0.83, metabolites were obtained and imported into MetaboAnalyst website for metabolic pathway analysis. All statistical analyses were performed using Graphpad Prism 8.0 and the metabolic analysis website.

Network pharmacology prediction

The SMILES structures of FZA identified in Section "Integrated analyses of the proteomics and metabolomics results" were retrieved from Pubchem database (https://pubchem.nc-bi.nlm.nih.gov/) and introduced into Swiss Target Prediction website to predict the potential targets of FZA. Next, Uniprot database (https://www.uniprot.org/) was used to obtain the standard gene symbols of all the target proteins corresponding to FZA. Then, Genes related to NSCLC diseases were collected from GeneCards, TTD, OMIM database (https://www.genecards.org/). In order to clarify the interaction between FZA target and NSCLC related target, the two targets were intersected and the Venn Diagram was drawn. Cytoscape 3.8.2 software (https://cytoscape.org/) was used to map the active ingredients-target network of FZA in the treatment of NSCLC. The PPI network based on STRING was constructed using the minimum required interaction score of 0.4. All target proteins regulated by FZA were then subjected to DAVID database for functional enrichment analysis including GO and KEGG. The filtering of retrieval results is with a threshold value of $p < 0.05$ and the top 20 pathways were screened out according to the number of enriched genes. The visual bar charts and bubble plots were drawn.

Measurement of intracellular glucose and lactate levels

NCl-H1299 and A549 cells were inoculated in 6-well plates with 5×10^5 cells/well overnight. After discarding the medium, cells were treated with different concentrations of FZA (50, 100, 200 μg/mL) and cultured for 24 h. Then, the medium was collected and centrifuged. The pH value of the medium was measured with supernatant. Three replicate groups were set up. The cells were collected by ultrasonic crushing, centrifuged at 8000 × *g*, 4 °C for 10 min, and the supernatant was taken for BCA protein quantification. According to the protocols of lactate assay kit and glucose kit, the OD values were determined by microplate reader. The lactate and glucose content were calculated and normalized.

Assessment of energy metabolites by GC-MS

A549 cells at logarithmic growth stage were seeded in 60 mm culture medium and incubated overnight. After that, the medium was discarded. Then, different concentrations of FZA (50, 100, 200 μg/mL) were added and the medium was removed after 24 h of treatment. Three replicate groups were set up. The cells were washed twice with PBS and quenched by adding 1 mL of 60% methanol containing 70 mM HEPES on dry ice (−50 °C). Furthermore, 500 μL of pre-cooled 75% methanol-MTBE (9:1) containing 1,2-^{13}C myristyl (5 μg/mL) was added and frozen in cold nitrogen for 3 min. The mixture was then thawed at 37 °C for 10 min and the process was repeated for three times. The samples were centrifuged at 18,000 rpm for 10 min. The supernatant was evaporated to dryness at 45 °C in a centrifugal concentrator (Thermo Fisher, San Jose, CA, USA). After drying, 30 μL of methoxyamine hydrochloride dissolved in pyridine (*w/v*, 10 mg/mL) was added and vortexed for 5 min. Then, the samples were shaken at a speed of 300 rpm for 1.5 h in a thermostatic oscillator at 30 °C. Subsequently, 30 μL of BSTFA (1% TMCS) was added and shaken for 30 min at 37 °C. After derivatization, the mixture was centrifuged at 18,000 rpm for 10 min and 50 μL supernatant was injected into the GC-MS. The analysis conditions were the same as described in Section "FZA regulated aerobic glycolysis through the PI3K/Akt-mTOR pathway".

Western blotting analysis

The treated cells were lysed with ice-cold cell lysis buffer containing protease and phosphatase inhibitor cocktail. Dissolved proteins were collected, and the debris was removed by centrifugation at 12,000 rpm for 10 min at 4 °C. The concentration of total protein was determined using the BCA protein assay kit. Equal amounts of lysate protein were electrophoresed by FuturePAGE (ACE, Nanjing, China). The separated proteins were transferred electrophoretically to PVDF membranes. The membranes were blocked with 5% BSA in tris buffer solution-tween (TBST) for 2 h and subsequently incubated overnight at 4 °C with primary antibodies. After washing with TBST, the membranes were incubated with HRP-conjugated Affinipure Goat Anti-Rabbit lgG(H + L) for 2 h at room temperature. Thereafter, reactive bands were visualized by the Chemidoc XRS+ Imaging System (Bio-Rad; Hercules, CA) using super ECL detection reagent (Yeasen, China) and analyzed by Image J software.

Statistics and reproducibility

All data was present as mean ± SD. Data between two groups was analyzed by Student's t-test, while one-way ANOVA was used to analyze data for more than two groups. Graphs were generated and statistically analyzed using GraphPad Prism 8 software. Significance is indicated as following: *, $p < 0.05$; **, $p < 0.01$; ***, $p < 0.001$. Data shown are representative of at least three independent experiments, including cell experiments, animal studies and blots.

Reporting summary

Further information on research design is available in the Nature Portfolio Reporting Summary linked to this article.

Data availability

All other data are available from the corresponding author (or other sources, as applicable) on reasonable request. The uncropped gel images have been present in Fig.S4 from Supplementary Information. The numerical source data behind the graphs in the manuscript can be found in Supplementary Data 1. The data of Components identified in FZA and differentially expressed proteins (DEPs) between model and FZA groups by proteomics are available from Supplementary Data 2. Mass spectrometry-based proteomics data are available at iProX (IPX0009455000).

Received: 20 June 2023; Accepted: 29 August 2024;
Published online: 11 September 2024

References

1. Sung, H. et al. Global cancer statistics 2020: GLOBOCAN estimates of incidence and mortality worldwide for 36 cancers in 185 countries. *CA Cancer J. Clin.* **71**, 209–249 (2021).
2. Singh, T., Fatehi Hassanabad, M. & Fatehi Hassanabad, A. Non-small cell lung cancer: Emerging molecular targeted and immunotherapeutic agents. *Biochim Biophys. Acta Rev. Cancer* **1876**, 188636 (2021).
3. Li, B., Zhang, X., Ren, Q., Gao, L. & Tian J. NVP-BEZ235 inhibits renal cell carcinoma by targeting TAK1 and PI3K/Akt/mTOR pathways. *Front Phamacol* **12**, 781623 (2021).
4. Liu, H., Liu, R., Hao, M., Zhao, X. & Li, C. Kinesin family member 3C (KIF3C) is a novel non-small cell lung cancer (NSCLC) oncogene whose expression is modulated by microRNA-150-5p (miR-150-5p) and microRNA-186-3p (miR-186-3p). *Bioengineered* **12**, 3077–3088 (2021).
5. Alsharairi N. A. Scutellaria baicalensis and their natural flavone compounds as potential medicinal drugs for the treatment of nicotine-induced non-small-cell lung cancer and asthma, *Int. J. Environ. Res. Public Health* **18**, https://doi.org/10.3390/ijerph18105243 (2021).
6. Xiao, Z. et al. Comprehensive TCM treatments combined with chemotherapy for advanced non-small cell lung cancer: A randomized, controlled trial. *Med. (Baltim.)* **100**, e25690 (2021).

7. Zhang, K., Liu, Y. S., Lin, X., Yang, J. Y. & Wu, C. F. Assessment of reproductive toxicity and genotoxicity of Aconiti Lateralis Radix Praeparata and its processed products in male mice. *J. Ethnopharmacol.* **275**, 114102 (2021).
8. Zhang, Q., Chen, X., Luo, Y. J., Ren, H. P. & Qiao, T. K. Fuzi enhances anti-tumor efficacy of radiotherapy on lung cancer. *J. Cancer* **8**, 3945–3951 (2017).
9. Zhang, F. Y. & Guo, S. C. Exploring the mechanism and experimental validation of Fuzi Lizhong Tang in treating gastric cancer based on network pharmacology and molecular docking. *Eur. Rev. Med. Pharm.* **27**, 9192–9204 (2023).
10. Wei, X. H. et al. Mahuang Fuzi Xixin decoction ameliorates allergic rhinitis and repairs the airway epithelial barrier by modulating the lung microbiota dysbiosis. *Front Microbiol* **14**, 1206454 (2023).
11. Chen, J. B. et al. Sini decoction inhibits tumor progression and enhances the anti-tumor immune response in a murine model of colon cancer. *Comb. Chem. High. T Scr.* **26**, 2517–2526 (2023).
12. Zhang, W. T. et al. Explore the mechanism and substance basis of Mahuang FuziXixin Decoction for the treatment of lung cancer based on network pharmacology and molecular docking. *Comput Biol. Med.* **151**, 106293 (2022).
13. Chen, G. Effects of Shenfu injection on chemotherapy-induced adverse effects and quality of life in patients with advanced nonsmall cell lung cancer: A systematic review and meta-analysis. *J. Cancer Res Ther.* **14**, S549–S555 (2018).
14. Ji, B. L., Xia, L. P., Zhou, F. X., Mao, G. Z. & Xu, L. X. Aconitine induces cell apoptosis in human pancreatic cancer via NF-κB signaling pathway,. *Eur. Rev. Med Pharm.* **20**, 4955–4964 (2016).
15. Feng, H. T., Zhao, W. W., Lu, J. J., Wang, Y. T. & Chen, X. P. Hypaconitine inhibits TGF-β1-induced epithelial-mesenchymal transition and suppresses adhesion, migration, and invasion of lung cancer A549 cells,. *Chin. J. Nat. Med.* **15**, 427–435 (2017).
16. Gao, F., Li, Y. Y., Wang, D., Huang, X. & Liu, Q. Diterpenoid alkaloids from the Chinese Traditional Herbal "Fuzi" and their cytotoxic activity. *Molecules* **17**, 5187–5194 (2012).
17. Jin, Z. Q. et al. Higenamine enhances the antitumor effects of cucurbitacin B in breast cancer by inhibiting the interaction of AKT and CDK2. *Oncol. Rep.* **40**, 2127–2136 (2018).
18. Zhang, W. et al. Aconiti lateralis radix praeparata as potential anticancer herb: Bioactive compounds and molecular mechanisms. *Front. Pharmacol.* **13**, 870282 (2022).
19. Zhang W. et al. Modulation of cellular metabolism and alleviation of bacterial dysbiosis by Aconiti Lateralis Radix Praeparata in non-small cell lung cancer treatment, *Phytomedicine* https://doi.org/10.1016/j.phymed.2023.155099 (2023).
20. Gonulalan, E. M. et al. Metabolomics and proteomics profiles of some medicinal plants and correlation with BDNF activity. *Phytomedicine* **74**, 152920 (2020).
21. Zhao, D., Xu, J. & Xiao, M. Application of metabolomics in research of traditional Chinese medicine. *Asia-Pac. Traditional Med.* **17**, 206–209 (2021).
22. Guijas, C., Montenegro-Burke, J. R., Warth, B., Spilker, M. E. & Siuzdak, G. Metabolomics activity screening for identifying metabolites that modulate phenotype. *Nat. Biotechnol.* **36**, 316–320 (2018).
23. Hasin, Y., Seldin, M. & Lusis, A. Multi-omics approaches to disease. *Genome Biol.* **18**, 83 (2017).
24. Zhu, Y. et al. New opportunities and challenges of natural products research: When target identification meets single-cell multiomics. *Acta Pharmaceutica Sin. B* **12**, 4011–4039 (2022).
25. Xia, L. et al. The cancer metabolic reprogramming and immune response. *Mol. Cancer* **20**, 28 (2021).
26. Vaupel, P. & Multhoff, G. Revisiting the Warburg effect: Historical dogma versus current understanding. *J. Physiol.* **599**, 1745–1757 (2021).
27. Xu, K. et al. Glycolysis fuels phosphoinositide 3-kinase signaling to bolster T cell immunity. *Science* **371**, 405-+ (2021).
28. Hosios, A. M. & Manning, B. D. Cancer signaling drives cancer metabolism: AKT and the Warburg effect. *Cancer Res.* **81**, 4896–4898 (2021).
29. Huang, R. et al. A review: PI3K/AKT/mTOR signaling pathway and its regulated eukaryotic translation initiation factors may be a potential therapeutic target in esophageal squamous cell carcinoma. *Front Oncol.* **12**, 817916 (2022).
30. Lien, E. C., Dibble, C. C. & Toker, A. PI3K signaling in cancer: Beyond AKT. *Curr. Opin. Cell Biol.* **45**, 62–71 (2017).
31. Hoxhaj, G. & Manning, B. D. The PI3K-AKT network at the interface of oncogenic signalling and cancer metabolism. *Nat. Rev. Cancer* **20**, 74–88 (2020).
32. Lee, J. H. et al. EGFR-phosphorylated platelet isoform of phosphofructokinase 1 promotes PI3K activation. *Mol. Cell* **70**, 197-+ (2018).
33. Düvel, K. et al. Activation of a metabolic gene regulatory network downstream of mTOR complex 1. *Mol. Cell* **39**, 171–183 (2010).
34. Chen, P., Liu, Y., Wen, Y. & Zhou, C. Non-small cell lung cancer in China. *Cancer Commun. (Lond., Engl.)* **42**, 937–970 (2022).
35. Peng L. et al. Real-world evidence of traditional Chinese medicine (TCM) treatment on cancer: A literature-based review. Evid. Based Complement. Alternat. Med. https://doi.org/10.1155/2022/7770380 (2022).
36. Liang L. et al. 'Reverse Warburg effect' of cancer-associated fibroblasts (Review), *Int. J. Oncol.* **60**, https://doi.org/10.3892/ijo.2022.5357 (2022).
37. Sun, L., Suo, C., Li, S. T., Zhang, H. & Gao, P. Metabolic reprogramming for cancer cells and their microenvironment: Beyond the Warburg Effect. *Biochim Biophys. Acta Rev. Cancer* **1870**, 51–66 (2018).
38. Qiu, L. et al. HBXIP regulates gastric cancer glucose metabolism and malignancy through PI3K/AKT and p53 signaling. *OncoTargets Ther.* **13**, 3359–3374 (2020).
39. Iksen, Pothongsrisit S. & Pongrakhananon, V. Targeting the PI3K/AKT/mTOR signaling pathway in lung cancer: an update regarding potential drugs and natural products. *Molecules*. **26**, 4100 (2021).
40. Cheng, G. et al. β-elemene suppresses tumor metabolism and stem cell-like properties of non-small cell lung cancer cells by regulating PI3K/AKT/mTOR signaling. *Am. J. Cancer Res*. **12**, 1535–1555 (2022).
41. Cai, S. et al. Optimization of purification process for total alkaloids from Aconiti Lateralis Radix Praeparata. *Chin. Tradit. Pat. Med.* **45**, 3023–3028 (2023).

Acknowledgements

This study work was supported by the National Natural Science Foundation of China (No. 82104688), Natural Science Foundation of Jiangsu Province of China (No. BK20190800), Natural Science Foundation of the Jiangsu Higher Education Institutions of China (19KJB360004), Natural Science Foundation of Nanjing University of Chinese Medicine (XPT82104688), and Postgraduate Research & Practice Innovation Program of Jiangsu Province (SJCX24_0900).

Author contributions

W.Z.: Conceptualization, Project administration, Funding acquisition, Methodology, Investigation, Writing—review & editing. S.C.: Methodology, Investigation, Formal analysis, Data curation, Writing—original draft. L.Q.: Investigation, Formal analysis, Data curation, Writing—original draft. M.D.: Investigation, Formal analysis. Y.F.: Investigation, Formal analysis. Z.L.: Methodology, Investigation. J.S.: Methodology, Formal analysis. L.D.: Conceptualization, Project administration, Supervision, Writing—review & editing.

Competing interests

The authors declare no competing interests.

Additional information

Supplementary information The online version contains supplementary material available at https://doi.org/10.1038/s42003-024-06801-6.

Correspondence and requests for materials should be addressed to Wen Zhang or Liuqing Di.

Peer review information : *Communications Biology* thanks Ajay Kumar and the other, anonymous, reviewer(s) for their contribution to the peer review of this work. Primary Handling Editors: Bibekanand Mallick and David Favero. A peer review file is available.